INTERNATIONAL JOURNAL FOR NUMERICAL METHODS IN FLUIDS, VOL. 4, 359–375 (1984)

ON THE ACCURACY OF BOUNDARY FITTED FINITE-DIFFERENCE CALCULATIONS

J. C. FERRERI* AND M. A. VENTURA*

Gerencia de Protección Radiológica y Seguridad, CNEA, Av. del Libertador 8250, (1429) Capital Federal, Argentina

SUMMARY

A description is given of the effects of the discretization of the domain of integration on the accuracy of the results obtained with boundary-fitted finite differences. Three-dimensional unsteady heat conduction problems and two dimensional Navier–Stokes equations are considered. Comparisons with analytic solutions are given for all cases. It is shown that grid shapes influence the accuracy of the results and quantitative error evaluations are provided for some interesting cases.

KEY WORDS Boundary-fitted Finite-differences Accuracy

INTRODUCTION

Grids of variable spatial step sizes are frequently employed in order to solve heat conduction problems in domains of complicated shapes or in zones of simple bodies where the temperature varies very rapidly ('boundary layers'). The most recent improvement in the finite-difference technique is the introduction of discrete co-ordinate transformations in order to obtain an automatic adaptation of the computing grid to the case of interest. In References 1–16 examples may be found concerning this technique, usually under the name of boundary-fitted finite differences and covering a vast field of applications of diverse complexity.

The literature does not usually include detailed discussions on the effect of the type or shape of the grid employed to fit the integration domain upon the accuracy of the results obtained. Since the present authors found systematic difficulties in applying some commonly employed co-ordinate transformations, they considered it would be interesting to show both qualitative and quantitative effects of the discretization employed on the accuracy of the results. The results shown could also be applicable to the finite element method when simple quadrilaterals, with the function specified at corners, are employed. Recent references[17,18,19] show that interest has arisen in obtaining quantitative criteria regarding the applicability of discrete techniques based on complete tests of accuracy with respect to analytical solutions.

The following paragraphs show the effect of the shape and size of the discrete cells employed to solve three-dimensional (3D) unsteady heat condition problems on the accuracy of the results obtained. Boundary conditions of the Dirichlet and Neuman type are considered. In the case of the Navier–Stokes equations boundary-fitted finite differences are employed in order to compute the flow in the cavity formed by two concentric cylinders. Comparisons with analytic solutions are performed for all cases.

---

* Member of Carrera del Investigador Científico del CONICET, Argentina.

0271–2091/84/040359–17$01.70

Received 3 August 1982
Revised 10 January 1983

EFFECT OF DISCRETIZATION ON THE ACCURACY OF RESULTS

3D unsteady heat conduction

Let us consider a grid adapted to a sphere of radius a, resulting from a discrete co-ordinate transformation.

The nodes in this grid correspond with the ones of the unit cube $0 \leqslant u \leqslant 1$, $0 \leqslant v \leqslant 1$, $0 \leqslant w \leqslant 1$, as sketched in Figure 1. When the transformation is specified by means of Laplace equations for the internal points of the sphere and of a uniform distribution on the sphere surface for the points on the cube faces, the distribution of points in two opposed sphere surface segments and a middle plane is shown in Figure 2, for an $11 \times 11 \times 11$ discretization.

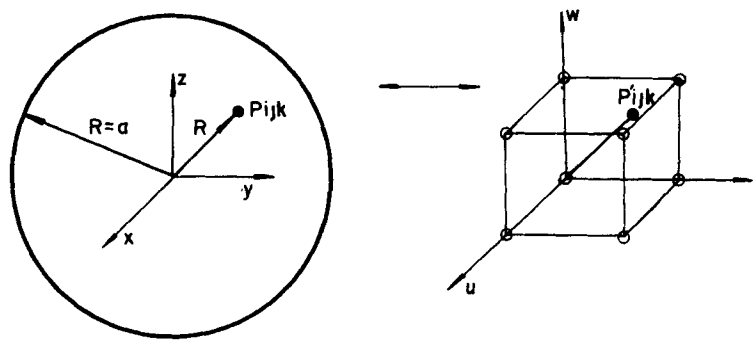

Figure 1. Definition of corresponding points in the physical and reference domains

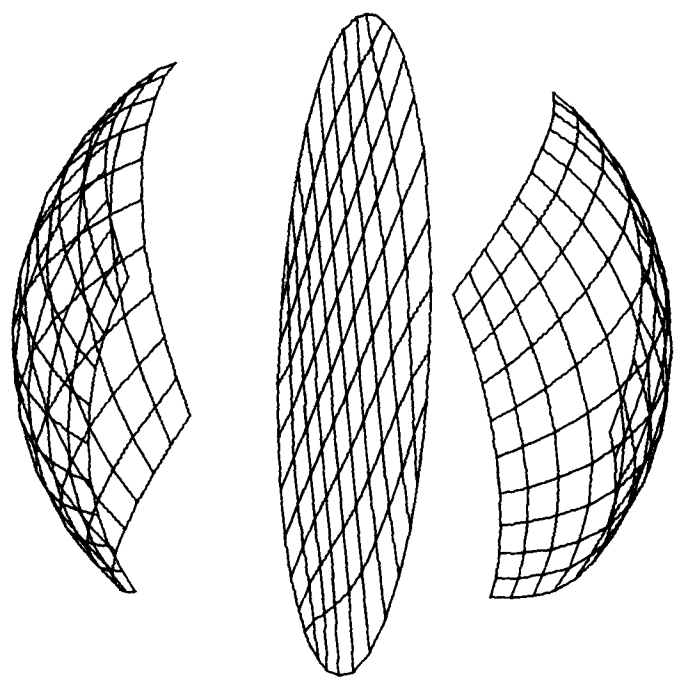

Figure 2. 3D representation of part of a grid adapted to a sphere

When a similar procedure is applied to a circular cylinder the results obtained are those shown in Figure 3 for a plane normal to the axis.

Figure 4 shows the grid in the case of a pyramidal frustrum with rounded edges. In heat conduction problems the use of grids of this type avoids discontinuities associated with the origin of co-ordinates which are always found in grids of the polar type, the latter being the natural ones for the cases shown in Figures 1 and 2.

On the other hand, non-polar grids have been frequently employed in the case of fluid flows[1] and, furthermore, allow for a simple treatment of the logic of the computer program.

However, there are problems for which is it difficult to decide whether or not a grid is adequate and, when the solution of the problem is unknown (obviously in the majority of the cases), one must choose among a type of discretization, like the one shown above, a grid of the polar type, like the one in Figure 5 with a particular treatment in its origin,[2,3] and a hybrid one with triangular and rectangular cells of the finite element type. The use of automatic grid generators presents problems as discussed by Hausling[4] and, for such reasons, the use of non-polar grids is sometimes advantageous.

Some limitations arising from the use of non-polar grids are shown below.

Uniformly heated bodies

Let us consider the mid plane normal to the axis of a circular cylinder uniformly heated by a hot environment. The boundary condition can be stated as:

$$\partial T/\partial n = -CT$$

Let us suppose that the initial temperature at the internal points is constant.

Because of symmetry, it is obvious that the temperature must be constant on the perimeter of this circle. In what follows, it is shown that the attainment of such a constant value is not possible if a non-polar grid is used. Figure 6 shows a hypothetical numbering in the vicinity of the boundary of the cylindrical surface.

A discrete representation of the former boundary condition at point 0, using a backward

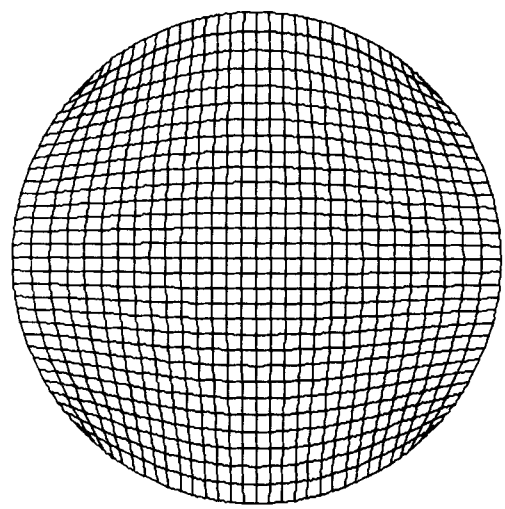

Figure 3. Cross-section of a grid adapted to a circular cylinder

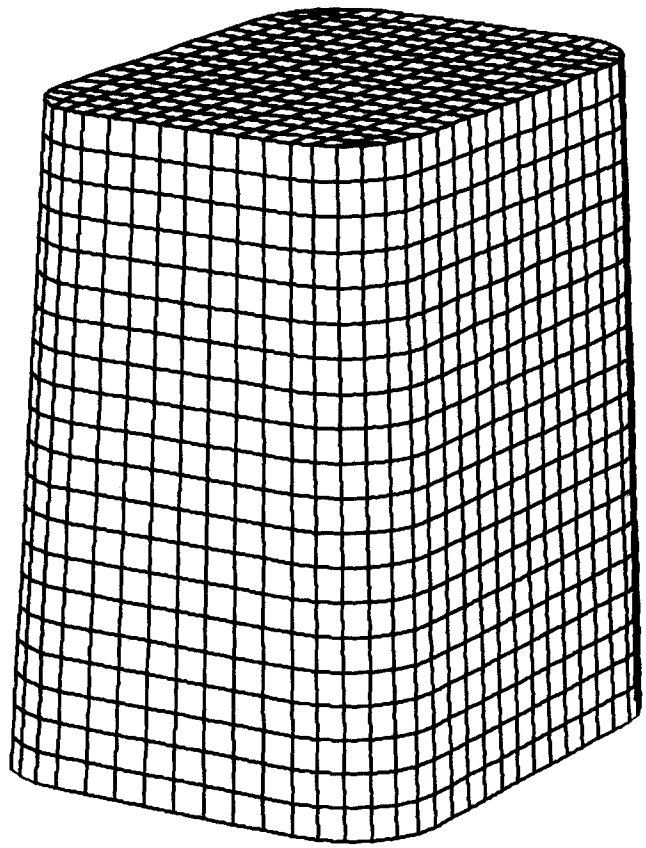

Figure 4. 3D representation of a grid adapted a pyramidal frustrum with rounded edges

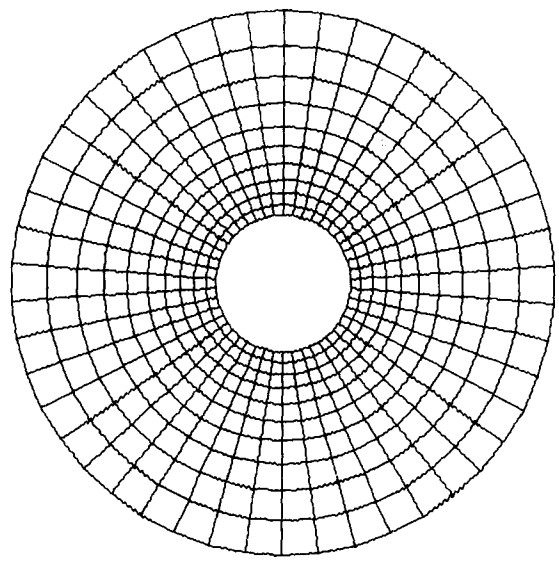

Figure 5. 'Polar' grid adapted to a circular cavity

first-order derivative for the internal point, may be stated as follows:

$$\mathrm{AUN}\,(T_0 - T_3) + \mathrm{AVN}\,(T_1 - T_2) = -CT_0$$

see Appendix I for the definitions of AUN and AVN.

If the desired temperature is constant at the surface (say T_s), then $T_0 \equiv T_1 \equiv T_2 \equiv T_s$; consequently,

$$T_s = \mathrm{AUN}\,T_3/(C + \mathrm{AUN})$$

since $T_3 = 1$ for $t = 0$ in all the internal points and C is a constant, then this identity holds if, and only if, AUN is independent of the point on the surface being considered. Of course AUN depends on the position of the points in the interior of the transformed domain; thus, the surface temperature will be constant if the grid points are uniformly distributed on concentric circumferences with their origin at the origin of the co-ordinates. Then, it became evident that, if the criterion of employing non-polar grids of the type herein considered is maintained, one must deal with some lack of uniformity in the solution at the surface.

An extreme case of symmetry and constancy of the temperature on a surface is that of an isotropic sphere uniformly heated from the environment.

In what follows a set of results is shown for the case in which the equation

$$\frac{\partial T}{\partial t} = \frac{\partial^2 T}{\partial x^2} + \frac{\partial^2 T}{\partial y^2} + \frac{\partial^2 T}{\partial z^2}$$

is solved in the interior of such sphere and subject to the boundary condition

$$\frac{\partial T}{\partial n} = -BiT$$

where $Bi = hk/D$ is the Biot number. The analytical solution can be found in Reference 20. Details of the methodology are given in Appendix I, although only for 2D.

The numerical procedure is explicit in time, involving a forward-Euler approximation of the time derivative. The temperature values at the internal points of the grid at time $t + \Delta t$

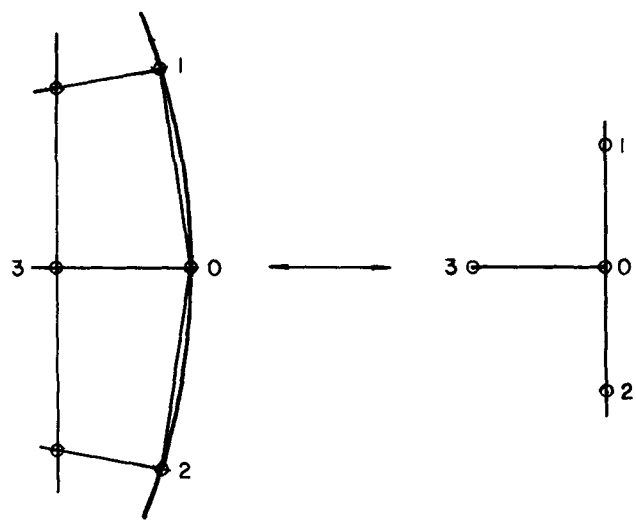

Figure 6. Numbering of a grid in the vicinity of a boundary

are obtained explicity from the values of T at time t, at both the internal and boundary points. It should be noted that the presence of the non-null cross derivatives involves the use of 19 points at time t in the 3D case.

In order to proceed to a new calculation step, boundary conditions must be applied at the grid points lying on the boundary. The simple example above shows the algebraic coupling of the nodes involved in the application of the boundary conditions. In the 3D case, five boundary nodes are coupled in the calculation of a new value. In order to avoid the use of a direct solver for this algebraic problem, an iterative, over-relaxation method was employed.

So, the procedure consisted in an explicit time advancement of the temperature at the internal points and in an iterative solution of the temperature at the surface. This iteration was performed until the solution converged to three significant digits.

Special attention was paid to the verification of the algebraic exactness of the solution in order to avoid further lack of uniformity. The closure of the system of equations on the boundary was sufficiently accurate in the cases under analysis.

Three similar grids were employed for the calculations, all of them fitted to the surface of the sphere (see Figure 2). They had $7\times7\times7$, $11\times11\times11$ and $17\times17\times17$ ($N_T = 343$, 1331 and 4913) points. The grid of reference was a unit cube and, therefore, the maximum distortions of the grid correspond with the vertices of the cube.

It seems convenient to give an idea of the global accuracy of the results obtained from the very beginning. The radial variation of the temperature, reduced by the centre temperature, is shown in Figure 7 for three values of the Biot number and for $t = 0{\cdot}15$. The particular values of Bi shown therewith are due to the fact that the tables of Carslaw and Jaeger[20] were employed for the analytical solution.

As can be seen from the Figure, the solution seems reasonably accurate, degrading when consideration is given to the points lying in the lines linking the centre of the sphere with the 'vertices' of the fitted grid. (These lines are termed 'diagonals' in Figure 7).

This Figure shows the results obtained with $N_T = 4913$ just for the case with $Bi = \infty$. As it can be observed, the results are almost coincident with the analytic ones. Similar results were obtained for $Bi = 116$; however, they are not shown in this Figure because they lie too close to the ones for $Bi = \infty$. The solution for $N_T = 4913$ was quite expensive in terms of computer time, and, for this reason, results for lower Bi were obtained only for smaller integration times; consequently, these results are not shown in Figure 7.

Figure 8 shows the percentage error for the solution at the centre of the sphere with respect to the analytic value as a function of the number of cells for two different values of Bi and for different times of integration. Thus, the error decreases as N_T increases.

As mentioned above, this type of grid imposes non-uniformity in the solution at the surface. Figure 9 shows the range of separation of the temperature at the surface with respect to the analytic value, as a function of time for different Bi and N_T. In this Figure it is evident that this difference is relatively smaller as Bi decreases; when Bi decreases, the temperatures, at constant time, are higher. This leads one to think that the magnitude of the difference is a function of the number of cells rather than one of the Biot number.

This figure shows little improvement in spite of a great increment of computational work. (i.e. considering $N_T = 4913$ instead of 1331 grid points). This fact can be attributed to one reason: consideration was just given to the maximum temperature difference in the whole surface without taking into account the spatial distribution. However, despite the improved accuracy of the calculations at internal points, the increase in accuracy at the surface points was not quite rewarding.

Figure 10 shows the mean square deviation of the temperature value with respect to the

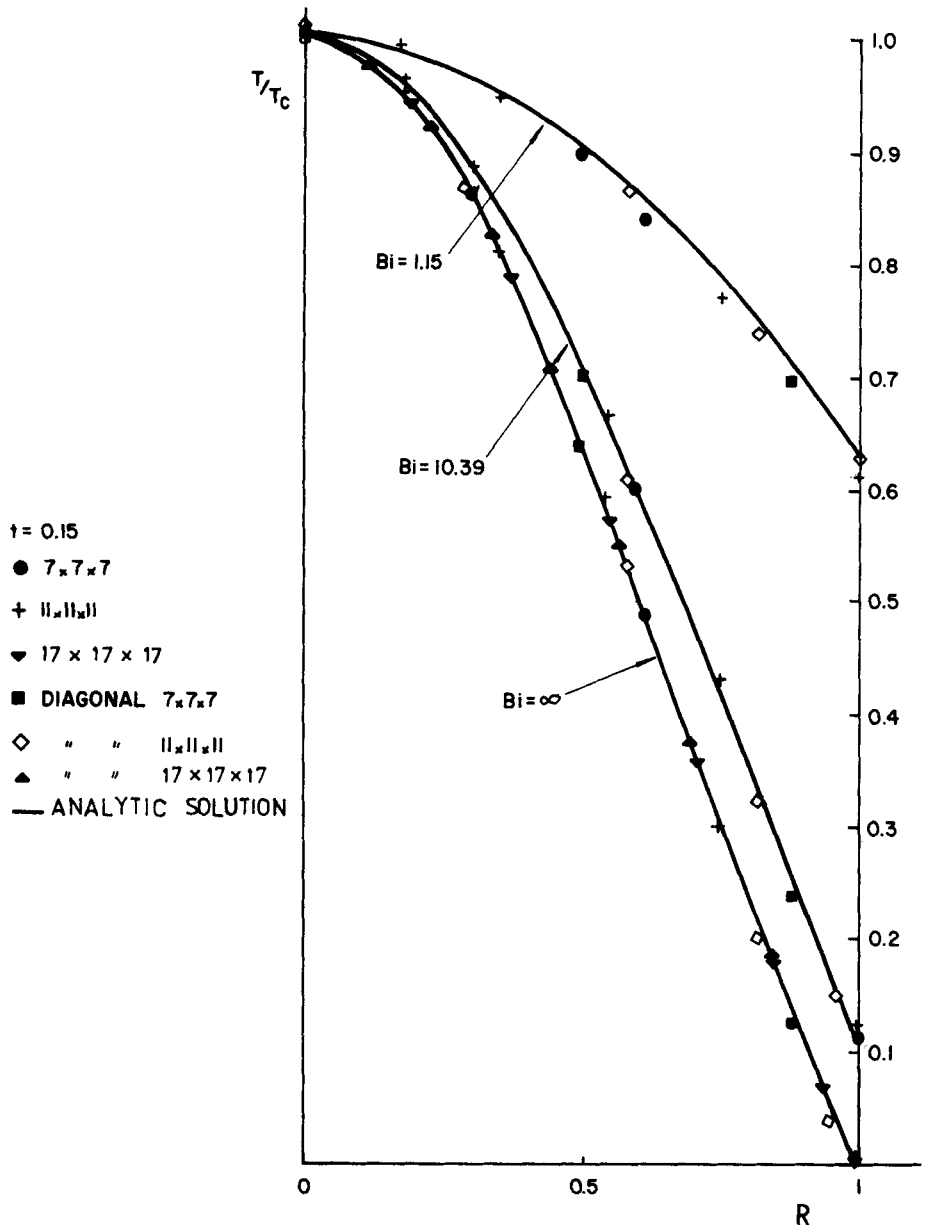

Figure 7. Radial distribution of reduced temperature in a uniformly heated sphere

analytic surface temperature for different Bi and N_T values. The definition of the percentage error there shown is:

$$\xi = \sum_{i}^{N_S} (T_i - T_{san})^2 / (N_S T_{san}^2) \times 100 \text{ per cent}$$

where N_S is the number of grid points lying on the surface. As can be seen, this measure of the error decreases as the cell number increases.

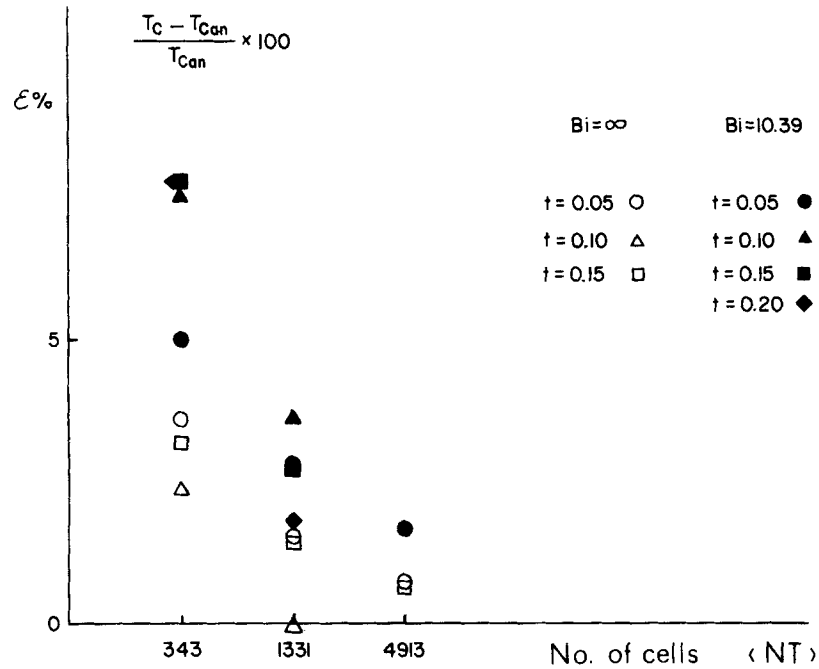

Figure 8. Error in the calculated temperature at the centre of a heated sphere

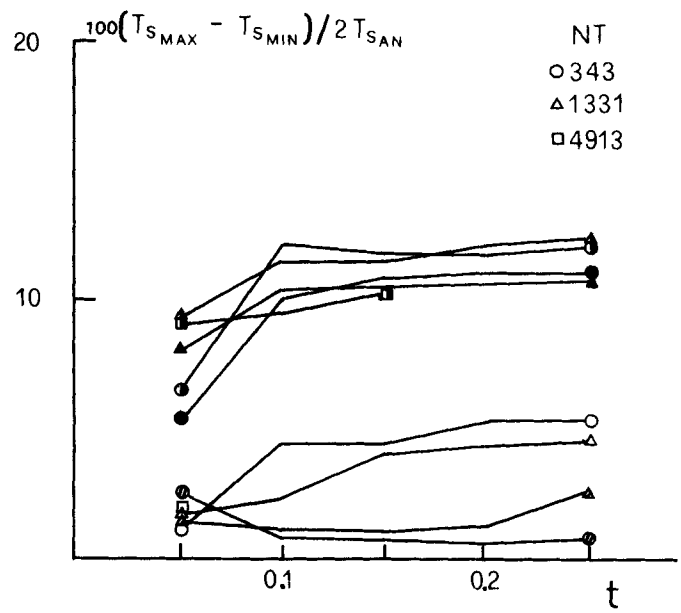

Figure 9. Maximum temperature difference at the surface of a heated sphere. Symbols: shaded: $Bi = 1$; open: $Bi = 10$, black: $Bi = 58{\cdot}9$; b & w: $Bi = 116$

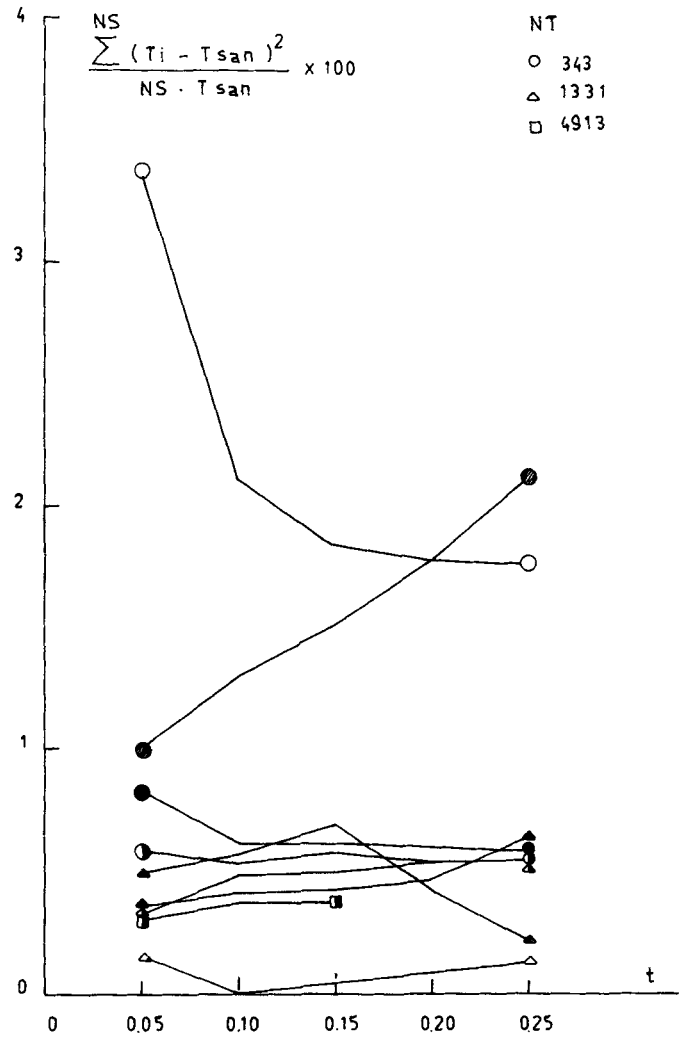

Figure 10. Error in the surface temperature in a heated sphere. Symbols as in Figure 9

Navier–Stokes equations

Let us consider an impulsively started flow between two concentric infinitely long cylinders. The equations governing the flow, in non-dimensional terms, are:

$$\frac{\partial \bar{u}}{\partial t} + (\bar{u} \cdot \nabla)\bar{u} = -\nabla P + \nu \nabla^2 \bar{u}$$

and

$$\nabla \cdot \bar{u} = 0$$

The boundary conditions employed in order to test the influence of the type of grid on the accuracy of the results include a free slip boundary with the normal component of the velocity vanishing at the wall. Note that we are dealing with boundary conditions which are not necessarily of the Neuman type. Details of the methodology can be found in Appendix II and those on the cases considered are shown below.

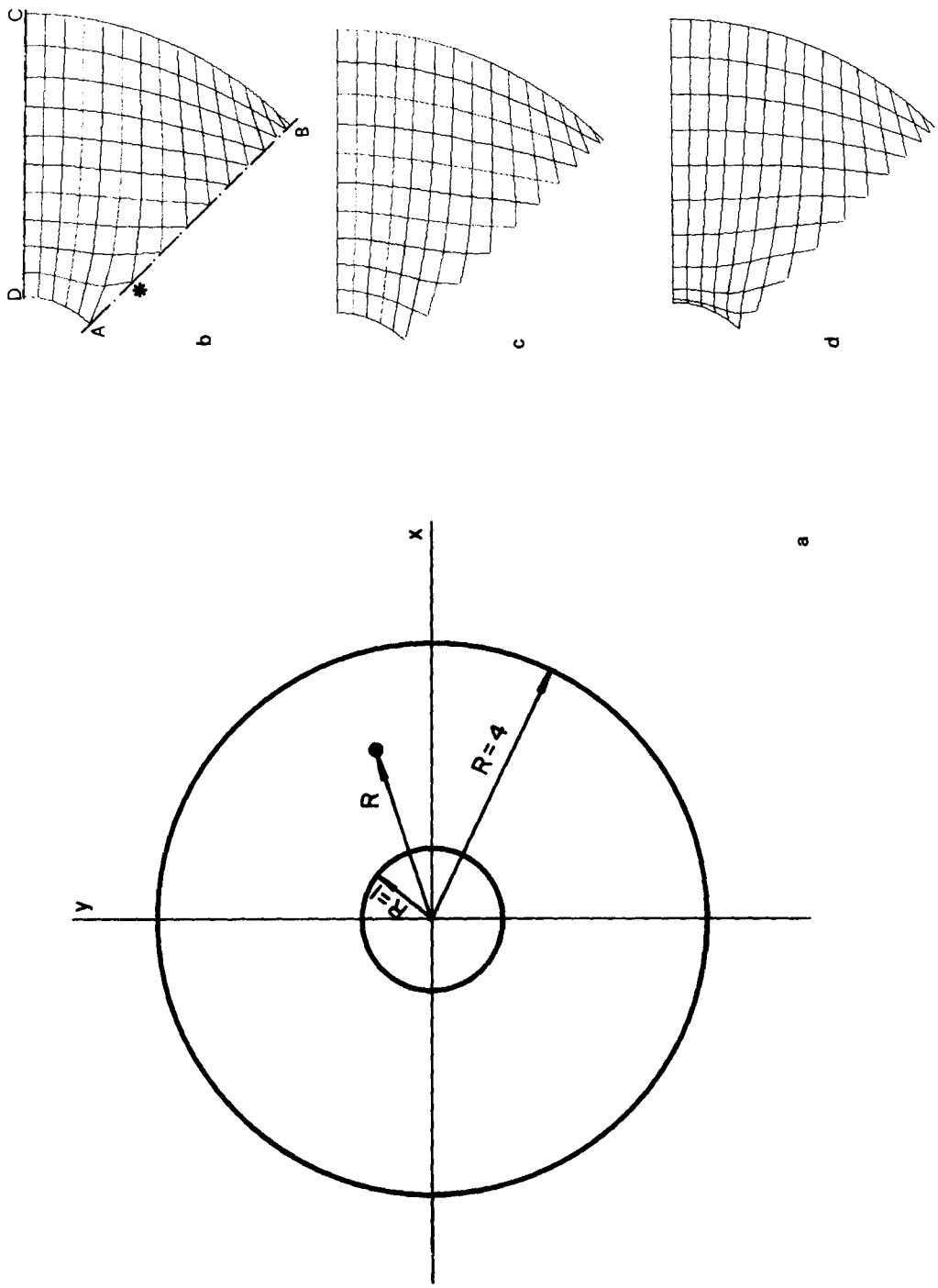

Figure 11. 'Non-plaar' grid adapted to the circular cavity

Table I. Grids employed for the circular cavity

	N_T	Number of points in external perimeter	Number of points in internal perimeter	Average $\Delta x \cdot \Delta y$
'Polar' grid Figure 5	517	47	47	~0·9
'non-polar' grids Figure 11	760	122	32	~0·9

Figure 11(a) shows the circular cavity considered. It was discretized with a 'polar' grid like the one in Figure 5 and also with a grid like the ones shown in Figures 11(b), (c), (d), the latter being the ones previously called 'non-polar' grids. The main characteristics for both types of grids are given in Table I

Calculations with the polar grid were performed considering that the solution is periodic. The set of cases considered was the following:

(i) A steady-state flow field, imposing the analytic solution as an initial velocity distribution,

$$u_n, u_t)_{R=1} = 0, \qquad u_t)_{R=4} = 1, \qquad u_n)_{R=4} = 0$$

where u_t is the velocity component tangential to the wall and u_n is the velocity component normal to the wall.

(ii) same as (i), except for

$$u_n)_{R=1} = 0, \qquad u_n)_{R=4} = 0, \qquad u_t)_{R=4} = 1$$

the values of $u_t)_{R=1}$ are obatained considering a free-slip boundary condition at the inner cylinder.

(iii) A steady-state flow field starting from rest,

$$u_t, u_n)_{R=1} = 0, \qquad u_t)_{R=4} = 1 \qquad u_n)_{R=4} = 0$$

The results obtained with the polar grid showed negligible errors in all cases. Calculations with the non-polar grid required a rather careful treatment regarding its shape, in order to obtain convergence in the pressure iteration. In order to obtain quantitative results, several non-polar grid shapes were employed. These are shown in Figure 11, although only partially considering their symmetry. Figure 11(b) is an annotated computer output plot. In this Figure, line BC represents the outer cylinder surface and line AD represents the inner cylinder surface. Segments AB and CD represent node lines showing the maximum and minimum grid distortions. Special consideration to these lines is given below.

Figure 11(b) corresponds to the grid obtained by solving Laplace equations (considering equal weights for all the points). With this grid, convergence of the pressure iteration could not be obtained, even when the time explicit advancement of velocity to $(n+1)\Delta t$ produced small variations with respect to the analytic solution corresponding to steady state. Non-convergence was caused by the poor accuracy of the solution at the point marked with an asterisk in Figure 11(b).

In order to improve the accuracy, the points were moved toward the centre of the domain by conveniently weighting the points as a function of their distance from the origin. A simple

way to do this is the one indicated by Amsden and Hirt.[23] The results obtained are shown in Figures 11(c) and (d). Figure 11(c) was obtained by attracting only those points on the diagonals of the hollow square domain used as a reference, whereas the grid shown in Figure 11(d) was obtained by similarly weighting all the points of the grid during the iteration and be defining the position of a point as the average of the position of the eight neighbouring ones. The position of the boundary was not allowed to iterate towards its final position as in Reference 23.

Not surprisingly, the solution was satisfactory only for those cases corresponding to the grids of Figures 11(c) and 11(d). As can be seen from the Figures the point responsible for the aforementioned difficulties is now closer to the inner surface. This fact, and a minor global grid distortion, lead to the elimination of convergence problems. The results obtained in this case were accurate, as is shown below.

For any unsteady methodology, a severe test involves considering the distribution corresponding to the steady flow field as the initial value (with rot $\bar{u} \neq 0$) and proceeding with the simulation.

If this initial distribution is maintained through a reasonable number of computational cycles, both the differential problem and its boundary conditions could be properly represented. Figure 12 shows the error of the numerical solution, as compared with the analytic solution, after 1600 cycles for the grid of Figure 11(c), along lines AB and CD. It is interesting to notice that the maximum error occurs at the closest point to the vertex of the inner square of the reference grid. This error is obtained at the very beginning of the calculation and, once attained, remains unchanged throughout cycle 1600 when the computation was discontinued.

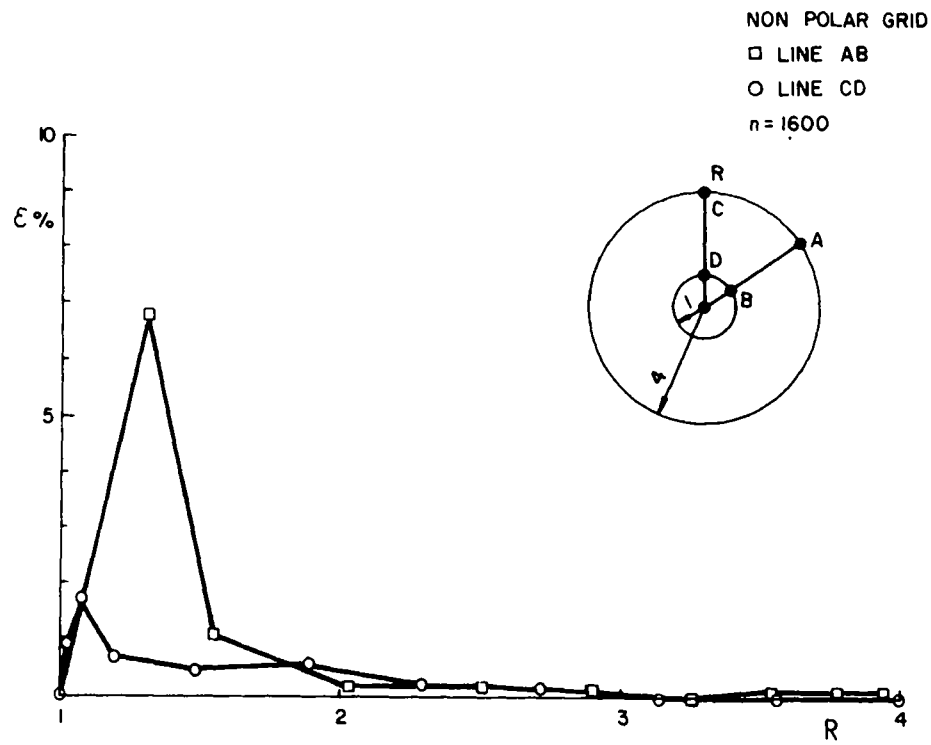

Figure 12. Error in the computed solution of NS equations, steady state solution, case (i)

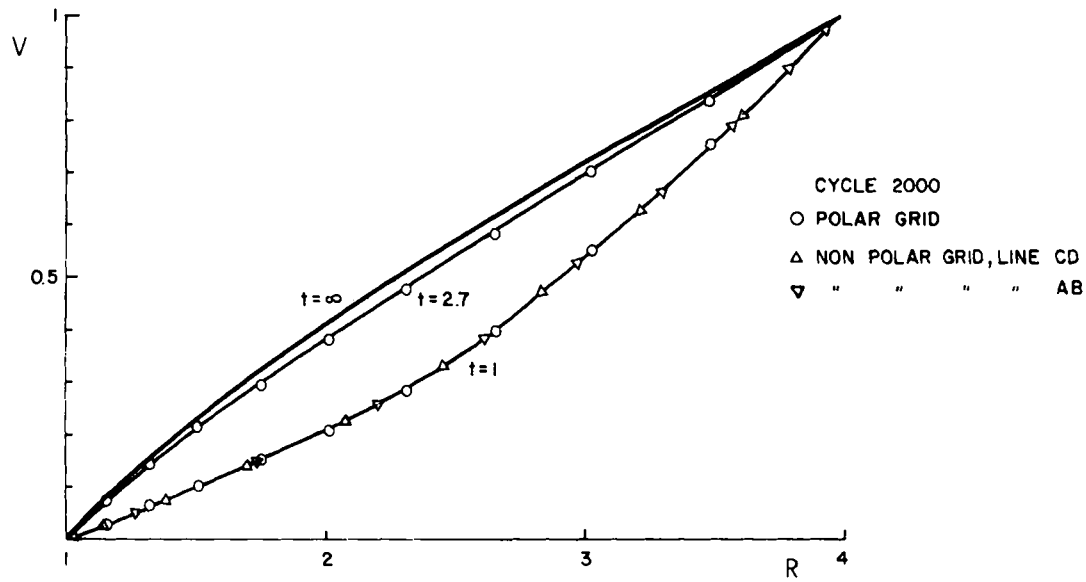

Figure 13. Comparison of computed solutions of NS equations, unsteady flow, case (iii)

The error in line CD is less significant, as shown in the same Figure. This fact can be attributed to the lower local grid distortion.

When the normal component of velocity is forced to vanish at the wall of the inner cylinder, the maximum error resulting from comparing the numerical solution with the analytic one does not grow above 0·5 per cent at the point marked with an asterisk. Finally, Figure 13 shows the comparison of the results, for the unsteady case, obtained with both grids, upon the completion of 2000 cycles. As can be seen, both results are indistinguishable.

DISCUSSION AND CONCLUSIONS

As shown above, it is possible to obtain accurate solutions in heat conduction problems and fluid flows in the interior of domains. From the reasoning and the calculations performed, it is evident that the selection of the grid brings along solutions that are frequently incompatible with the physical problem, especially if the selected grids are not uniform near the boundaries of the domain. Some problem cases are more sensitive than others to this lack of uniformity and their solution, under certain circumstances, may be unacceptable. The method used in solving 3D heat condition problems in the sphere showed the posssibility of obtaining results with great computational simplicity. It also served to avoid singularities at the origin, although at the cost of obtaining non-uniform temperatures.

The error is smaller as Bi decreases and this is due to the smoothness of the solution. An increase in the number of points in the grid does not necessarily improve the accuracy of the solution in terms of non-uniformity at the surface. This is due to a greater grid distortion and, in turn, as shown in Appendix I, the error can grow without limit. This error growth is associated with the vanishing of the Jacobian of the transformation in this cell. It can be said that a reasonable number of points, in the case of heat conduction in the interior of a sphere, must be of the order of 10^3, assuming they are adequately distributed.

In the case of Navier–Stokes equations, it is more difficult to reach a solution if the grid is

not adequately specified. For the flows considered herein, a reasonable 'radius' for the first nodal line should not exceed the inner cylinder radius by more than 5 per cent.

The imposition of free-slip boundary conditions notably eases the attainment of solutions. In those cases in which it is hard to specify whether a given lack of uniformity in the solution is due to the grid or to the physical problem, it would be difficult, in general, to choose any grid. The generation and the treatment of the grids herein considered are simple. This makes the grids quite useful as an alternative for checking different results. The distortion of the regular domain associated with the generation of the 'non polar' fitted grid increases with the number of grid points. This distortion usually causes the alignment of the consecutive sides of a quadrilateral, leading to an increase of the truncation error (see Appendix I). This problem can be avoided in this and other similar grids by carefully checking the maximum value that any internal angle of any quadrilateral could attain. Similar controls are typical in the finite element method.

The results obtained emphasize the need for an adequate calibration of the numerical schemes along with the grids employed.

ACKNOWLEDGEMENTS

The authors are grateful to Dr. P. M. Gresho and to the referees who kindly pointed out some suggestions, improving this paper.

APPENDIX I

The solution of a partial differential equation (PDE) with boundary-fitted finite differences is well known and consists in the transformation of the original PDE into another equation, usually more complicated, but referred to a space domain which is discretizable in regular cells.

The equation

$$\frac{\partial T}{\partial t} = \nabla^2 T$$

considering for simplicity the plane case, is expressed in the form:

$$\frac{\partial T}{\partial t} = \mathrm{AUU}\,T_{uu} + \mathrm{AUV}\,T_{uv} + \mathrm{AVV}\,T_{vv} + \mathrm{AU}\,T_u + \mathrm{AV}\,T_v$$

with

$$\mathrm{AUV} = u_x^2 + u_y^2 \qquad \mathrm{AU} = u_{xx} + u_{yy}$$
$$\mathrm{AUV} = 2(u_x v_x + u_y v_y), \qquad \mathrm{AV} = v_{xx} + v_{yy}$$
$$\mathrm{AVV} = v_x^2 + v_y^2$$

The boundary condition:

$$\frac{\partial T}{\partial n} = -BiT$$

is expressed as:

$$\mathrm{AUN}\frac{\partial T}{\partial u} + \mathrm{AVN}\frac{\partial T}{\partial v} = -BiT$$

The coefficients of the transformation are evaluated at grid nodes by means of second-order centred finite differences. At the boundaries of the domain, second-order backward

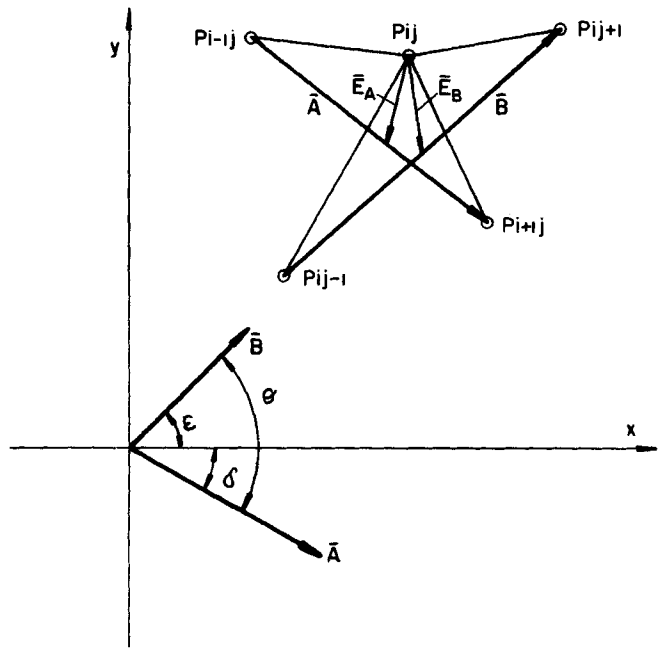

Figure 14. Definitions for truncation error analysis

or forward finite differences are used. An explicit forward discretization is employed for the time derivative.

The expressions for AUN and AVN are:

$$\mathrm{AUN} = n_x u_x + n_y u_y$$
$$\mathrm{AVN} = n_x v_x + n_y v_y$$

where n_x and n_y are the components of the unit vector normal to the surface. Algebraic details for obtaining these expressions can be found in Reference 5.

The truncation error of the expression for the normal derivative is of particular importance and is analysed below.

Fiora[21] showed that the truncation error for the first derivation is a function of the local distortion of the grid. Let us consider Figure 14. Fiora[21] obtained:

$$\left.\frac{\partial F}{\partial x}\right|_{P_{ij}} = -\left(\frac{\sin\delta}{A\sin\theta}\frac{F_{i+1\,j}-F_{i-1\,j}}{2} - \frac{\sin\varepsilon}{B\sin\theta}\frac{F_{i\,j+1}-F_{i\,j+1}}{2}\right)$$
$$\leqslant \frac{1}{\sin\theta}\left(C_1A^3+C_2B^3\right)+\frac{C}{\sin\theta}(E_A+E_B),$$

with a similar expression for $\left.\dfrac{\partial F}{\partial y}\right|_{P_{ij}}$

When the grid is orthogonal and equidistant, $\delta = \pi/2$, $\varepsilon = 0$, $A \cong \Delta x$ and $B \cong \Delta y$; then $E_A = 0$, $E_B = 0$ and $\theta = \pi/2$. In this case, this expression is reduced to the usual centred-error formula. If n_x and n_y are assumed free of error, then the truncation error of the normal derivative arises without difficulty. If θ tends to zero (i.e. two lines almost coincident), the

error grows without limits. In this case, the Jacobian of the transformation tends to zero and the transformation becomes singular. Furthermore, the error is proportional to the eccentricity of the point considered, measured by E_B and E_A. This eccentricity is representative of the amount of grid distortion.

APPENDIX II

In order to solve the Navier–Stokes equations in terms of primitive variables, a staggered grid, like the one shown in Figure 15 for the regular grid, is employed. The methodology adopted is a generalization of the SOLA algorithm[22] in order to consider discrete coordinate transformations.

Thus, the Navier–Stokes equations are explicitly advanced to time $(n+1)\Delta t$ and result in:

$$u_{n+1} = u_n + \Delta t(-\mathrm{FUX} - \mathrm{FUY} - \mathrm{DPDX} + \mathrm{VISX})$$

and

$$v_{n+1} = v_n + \Delta t(-\mathrm{FVX} - \mathrm{FVY} - \mathrm{DPDY} + \mathrm{VISY})$$

The advective terms are considered in a non-conservative form and are written, for example, as follows:

$$\mathrm{FUX} = \mathrm{AUX}_{ij} u_{ij}(u_{i+1\,j} - u_{i-1\,j})/2 + \mathrm{AVX}_{ij} u_{ij}(u_{i\,j+1} - u_{i\,j-1})/2$$

where the coefficients are defined as:

$$\mathrm{AUX} = u_x, \qquad \mathrm{AVX} = v_x$$

The diffusive terms are written in a form similar to the ones considered in Appendix I.

The terms which originated from the pressure variations, for example DPDX, are written as:

$$\mathrm{DPDX} = \mathrm{AUX}_{ij}(P_{i-1\,j-1} + P_{i-1\,j} - P_{i\,j-1} - P_{ij})/2 + \mathrm{AVX}_{ij}(P_{i-1\,j-1} + P_{i\,j-1} - P_{i-1\,j} - P_{ij})/2$$

The remaining terms are considered in the same way.

The values obtained by advancing the Navier–Stokes equations do not necessarily satisfy

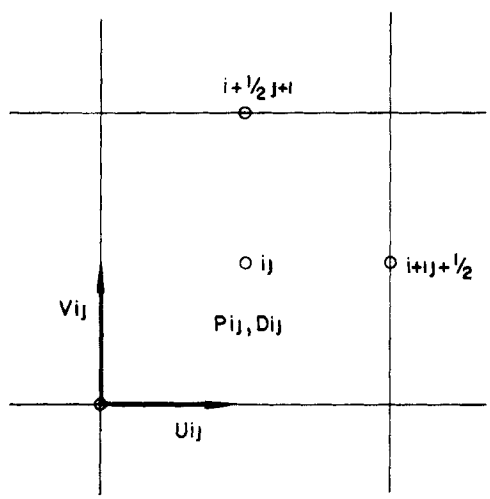

Figure 15. Definition of variables in the staggered grid for NS equations

the condition of zero-flow divergence. In order to satisfy this condition, an iterative procedure, as described below, is employed.

(i) The discrete analogue of cell divergence is obtained as follows:

$$D_{ij} = \mathrm{BUX}_{ij}(u_{i+\frac{1}{2}j} - u_{i-\frac{1}{2}j}) + \mathrm{BUY}_{ij}(u_{ij+\frac{1}{2}} - u_{ij-\frac{1}{2}}) + \mathrm{BVX}_{ij}(v_{i+\frac{1}{2}j} - v_{i-\frac{1}{2}j}) + \mathrm{BVY}_{ij}(v_{ij+\frac{1}{2}} - v_{ij-\frac{1}{2}})$$

(ii) The pressure in the cell is modified in order to force this divergence to be zero:

$$p_{ij}^{(k+1)} \leftarrow p_{ij}^{(k)} - \frac{\omega}{2\,\Delta t} \Big/ (\mathrm{BUU}_{ij} + \mathrm{BVV}_{ij})$$

(iii) Velocities are accordingly updated as follows:

$$u_{i+1j+1}^{(k+1)} \leftarrow u_{i+1j+1}^{(k)} + C(\mathrm{AUX}_{i+1j+1} + \mathrm{AVX}_{i+1j+1})$$
$$u_{i+1j}^{(k+1)} \leftarrow u_{i+1j}^{(k)} + C(\mathrm{AUX}_{i+1j} - \mathrm{AVX}_{i+1j})$$
$$u_{ij+1}^{(k+1)} \leftarrow u_{ij+1}^{(k)} + C(-\mathrm{AUX}_{ij+1} + \mathrm{AVX}_{ij+1})$$
$$u_{ij}^{(k+1)} \leftarrow u_{ij}^{(k)} + C(-\mathrm{AUX}_{ij} - \mathrm{AVX}_{ij})$$

with $C = \Delta t\, \delta P_{ij/2}$; the coefficients defined as BUV, etc., are the same as those shown as AUV, etc., but evaluated at cell centres. Similar expressions are written for v_i.

The algorithm is repeatedly applied until all D_{ij} lie below a given limit of tolerance. The boundary conditions are applied after each sweep through the complete field.

In the case of slipping walls, the expression:

$$\bar{v}_{\mathrm{B}} = \bar{v}_{\mathrm{A}} - (\bar{v}_{\mathrm{A}} \,.\, \bar{n})\bar{n}$$

is applied, where $\bar{v}_{\mathrm{B}}$ are the corrected velocities at the boundary including the zero normal component, $\bar{v}_{\mathrm{A}}$ is the value of $\bar{v}$ in the interior adjacent node after the pressure iteration and $\bar{n}$ is the outer normal vector evaluated at the boundary.

REFERENCES

1. W. E. Pracht and J. U. Brackbill, *LA-6342*, Los Alamos Scient. Lab., 1976.
2. W. T. Sha and J. F. Thompson, *Nureg/CR-0001*, ANL-78-1, Argonne Nat. Lab., 1978.
3. C. J. Chen, T. H. Hien, W. T. Sha, J. H. Kim and B. R. Sehgal, *Trans. A.N.S.*, **38,** 324, (1981).
4. H. J. Haussling, *Journal of Comp. Physics*, **30,** 107–124 (1979).
5. J. Fiora and J. C. Ferreri, *Lat. Am. J. of Heat & Mass Transf.* **2,** 29–44 (1978).
6. J. F. Thompson, F. C. Thames and C. W. Mastin, *Journal of Comp. Physics*, **15,** 299–319 (1974).
7. T. Gal-Chen and R. C. J. Sommerville, *Journal of Comp. Physics*, **17,** 276–310 (1975).
8. J. F. Thompson, F. C. Thames and C. W. Mastin, *Journal of Comp. Physics*, **24,** 274–302 (1977).
9. D. E. Potter and G. H. Tutle, *Journal of Comp. Physics*, **13,** 483–501 (1973).
10. P. R. Eiseman, *Journal of Comp. Physics*, **33,** 118–150 (1979).
11. P. C. M. Lau, *Int. J. Numer. Methods Eng.*, **14,** 791–812 (1979).
12. P. C. M. Lau, *Journal of Comp. Physics*, **32,** 325–344, (1979).
13. P. C. M. Lau, *Proc. of Third Int. Conf. in Australia on Finite Element Methods*, The University of South Wales Australia, 683–698 (1979).
14. L. Kosleelainen, in R. H. Lewis and K. Morgan, Eds, *Numerical Methods in Thermal Problems*, Pineridge Press, 1979, pp. 31–37.
15. S. R. Robertson, *Numerical Heat Transfer*, Vol. 2, 1979, pp. 61–80.
16. A. K. Agrawal and R. S. Peckover, *CLM-R209*, Culham Lab., UKAEA, 1980.
17. A. D. Solomon and D. G. Wilson, *ORNL/CSD*-65-1980.
18. E. Krause, *Computes and Fluids*, **8,** 31–57 (1979).
19. P. M. Gresho and R. L. Lee, *Computers and Fluids*, **9,** 223–253 (1981).
20. H. S. Carslaw and J. C. Jaeger, *Conduction of Heat in Solids*, Oxford, 1959.
21. J. A. Fiora, *Trabajo de Seminario*, Dto. Matemáticas, U.B.A. Argentina, 1978.
22. C. W. Hirt, B. D. Nichols and N. C. Romero, *VC34 and VC79s*, Los Alamos Scient. Lab., 1975.
23. A. A. Amsden and C. W. Hirt, *Journal of Comp. Physics*, **11,** 348–359 (1972).